Mixing effectiveness of fractal grids for inline static mixers

C.J. Coffey[1] , G.R. Hunt[1], R.E. Seoud[2] and J.C. Vassilicos[2]

1. Environmental and Industrial Fluid Mechanics Group
Department of Civil and Environmental Engineering

2. Turbulence, Mixing and Flow Control Group
Department of Aeronautics

Imperial College London,
London, SW7 2AZ, UK.

August 20, 2007

Abstract

The mixing and drag performances of two slightly different fractal grids (FG) and of two unoptimised pattern-enhanced fractal grid (PEFG) have been compared with those of a commercially available top-performance industrial mixing element (refered to as CSM for Current Standard of Mixing) and a regular turbulence-generating grid. A dye-attenuation technique was used to make synoptic and non-intrusive measurements of the concentration field downstream of each mixing element in a water flume at the Department of Civil Engineering. Drag measurements were made in the Donald Campbell wind tunnel of the Department of Aeronautics.

A key issue which arose from these Proof of Concept experiments is the importance for mixing of the mode of release. Within the present report's tight time and resource constraints, only pointwise continuous releases have been considered, upstream and downstream of the mixing elements. The results presented here have therefore much potential for improvement by designing optimal modes of release, perhaps depending on application. These results show that the FG and CSM elements generate comparable near and far field mixing in terms of local concentration values and in terms of single Coefficient of Variance (CoV) values. However these values are typically significantly higher for the FG elements. The PEFG1 element generates lower values and therefore better mixing than the FG both in the near and far fields, and in the near field it returns values nearly identical to the CSM. The PEFG2 element improves even further by mixing better than both FG and the CSM elements in the near field and mixing equally to the CSM in the far field.

In terms of spatial distribution of mixing the FG and the PEFG elements keep the mixing activity and the concentration field away from the walls, which is not the case of the CSM element. Furthermore, the normalised drag of the higher (FG2) and lower (FG1) blockage FG elements is lower than that of the CSM element by about 10% and 30% respectively, implying significant reductions in power losses. The normalised drag of the PEFG1 element is less than that of the PEFG2 element, and the normalised drag of the PEFG2 element is only 5% higher than that of the CSM, which means hardly any difference in drag when the mean flow is of the order of 10m/s or less (*i.e.* over the typical velocity range expected in practical applications).

In terms of concentration profiles, the CSM element achieves in the far field more spatial homogeneity than the FG elements but very comparable homogeneity to the PEFG elements. However, the CSM achieves this homogeneity by deviating parts of the flow towards the walls of the flume (or inline static mixer) in the near field, an occurrence which might be undesirable in some applications where the substances to be mixed are highly corrosive or persistently and/or recurrently hot. The fractal grids mix by generating high levels of turbulence (several times higher than regular turbulence-generating grids) for relatively low levels of blockage (and therefore low levels of drag and power losses) without brading different parts of the flow together, which is what the CSM mixer attempts to do with the result of throwing fluid at the walls. Hence, the pattern enhanced fractal grids can mix effectively and over short streamwise

distances. Furthermore, they do so by keeping the substances to be mixed clear of the walls.

The regular turbulence-generating grid mixes less well both in the far and near fields and less effectively (in terms of pressure drop and drag) than the CSM element and than all our FG and PEFG elements for all releases tried here.

The most impressive results are obtained when elements are combined. The combination PEFG2-CSM (PEFG2 placed upstream of CSM) mixes several times better than the combination CSM-CSM and than all individual CSM, FG and PEFG elements. This combination generates very good homogeneity of concentration fields and very high streamwise rates of decrease of CoV and particularly small CoV values as a result. Therefore, such combinations and optimisations of PEFG and FG single elements offer the very tangible possibility of setting an entirely new standard for mixing!

Quite importantly, this Proof of Concept study has confirmed the roles for mixing effectiveness of two of the main design parameters of the fractal grids: the thickness ratio t_r and the blockage ratio σ *which can be changed independently.* The turbulence intensity generated by a fractal element increases with t_r and, in agreement with consequent expectations, our measurements suggest that the CoV values are also increasing functions of t_r. The drag increases nonlinearly with σ, and our measurements have indeed confirmed that the drag on the low blockage ratio FG is much less than the drag on the high blockage ratio FG. The two FG elements which have been constructed for this study are fractal square grids and may look very similar to the untrained eye. However, their small differences have significant effects both on drag and on mixing, and the design of these very sensitive differences and of the resulting FG and PEFG elements has not been optimised, thus leaving tremendous scope for improvement. One may, for example, design low-σ (*i.e.* low drag) high-t_r (*i.e.* low CoV) fractal grids and work out the optimal sunstance release modes as well as, perhaps, optimal ways to combine fractal grids with each other and with CSM elements. There are also other design parameters which one can experiment with, such as those which characterise the differences between FG and PEFG, those which determine the distance from the grid where the turbulence intensity peaks, and many other patterns, beside the squares used here, which can be used for the design of fractal grids. There are therefore limitless possibilities and potential opportunities for effective mixing engineering and design which need to be explored. In addition, there is no reason to confine the scope of applications to static mixers; developments of fractal dynamic mixers may also be considered.

Along with this potential to set a new mixing standard over a broad range of mixing applications, the conclusion of this Proof of Concept report is that fractal grids in their current shape and form are very competitive mixing element products by comparison to commercially available top-performance industrial mixing elements.

1 Introduction

Research over the past ten years on fractal-generated turbulence pioneered and much of it carried out by Vassilicos's Turbulence Mixing and Flow Control Research Group (which moved from Cambridge to Imperial College London in January 2001) has now culminated in the clear identification of the geometrical parameters fully characterizing fractal grids and in the discovery of how these parameters determine and control turbulence excited in the lee of such grids (see Hurst & Vassilicos 2007 and references therein to earlier works). Hurst & Vassilicos (2007) tested in two different wind tunnels 21 different fractal grids pertaining to 3 different fractal families as well as a couple of regular mesh grids for comparison; Seoud & Vassilicos (2007a,b,c) and Mazellier *et al.* (2007a,b) made extensive further measurements on some of these grids. Broadly speaking, the main results which are pertinent to this report may be summarised as follows:

1. Fractal grids result in up to 3 times higher turbulence intensities than regular grids in the downstream region where turbulence is approximately homogeneous with about 30% less blockage ratio.

2. *Fractal grids offer the unprecedented possibility to independently control pressure drop and turbulence intensity.* It is therefore possible to tune them as very efficient mixers if pressure drop is made low by lowering blockage ratio whilst making turbulence intensities high by increasing the thickness ratio t_r between successive fractal iterations. Alternatively, it may be possible to tune them as silent airbrakes if the pressure drop is made high and turbulence intensity low.

3. The homogeneity of the turbulence downstream from fractal grids is to a great extent controlled by the fractal dimension D_f of the grid perimeter. Maximal, and in fact satisfactory, homogeneity is achieved when D_f takes the maximum possible value $D_f = 2$. Of the three families of fractal grids tested, the one which generates the most homogeneous downstream turbulence is the family of fractal square grids.

4. For fractal grids developed from closed contours (*e.g.* squares) a large-scale oscillation manifests itself immediately downstream (R.E. Seoud has also observed this from preliminary visualisations made for this present project in January 2007) which progressively breaks down into turbulence bursts as it is advected further downstream to eventually produce a peak of turbulence intensity at a distance x_{peak} from the grid which depends on the largest scales of the grid and on the size of the tunnel. This peak distance x_{peak} is a very sensitively controllable parameter but is nevertheless independent of flow rate. *Indeed, mean flow profiles in various directions are also found to be independent of flow rate when normalised by the upstream mean flow velocity.* Beyond this peak position the turbulence decays freely but in a way that is qualitatively, as well as quantitatively, different from any turbulence decay previously thought of or observed in experiments and simulations since the subject started in the first quarter of the 20th century: the turbulence decays exponentially (which means slowly to start with and eventually fast) with both macro and micro flow length-scales constant during decay!

It is on some of these results which the motivation for the proposed work rests. It may be worth repeating that, *as a consequence of the possibility to independently tune turbulence intensity and presure drop across fractal grids, a specific fractal grid can be chosen to yield desired results.* The example most relevant to one of the longer term objectives of the present project is to evolve a fractal grid design which acts as a particularly efficient mixer *for a broad range of conditions taking advantage of the fact that the mixing is effectively the same for a broad range of flow rates.* For an efficient mixer, one requires a low pressure drop (and hence low energy loss) to drive the flow across the grid, yet high turbulent intensities. Quite uniquely, fractal grids can achieve this previously contradictory double goal.

2 Methodology

Measurements were conducted in a recirculating flume that allowed a horizontal velocity of 5–50 cms^{-1} to be generated. A glass-sided test section was placed in the flume (of square cross section 20 cm x 20 cm and length 2 m), into which the fractal grids and CSM element could be fixed as their sides are also about 20 cm wide. Neutrally-buoyant dye was continuously released from a point source, driven by a constant head, at various points in the test section (both upstream and downstream of the grids) through a circular nozzle of diameter 1 mm. Care was taken to ensure the release velocities of the dye were of the order of the mean flow velocity so that the release could be considered passive (the velocity of the release was typically less than 1 cms^{-1}).

The flow was visualised using a dye-attenuation technique. The flow was backlit using a diffuse light source, and a CCD camera was used to measure the intensity of the light passing through the test section. This light was attenuated by any dye in the test section. Thus, by measuring this attenuation, the depth-averaged concentration field could be inferred. The advantage of this technique is that it allowed non-intrusive synoptic measurements of the concentration in the region of interest. See Hacker *et al.* (1996) and Cenedese and Dalziel (1998) for further details on this method.

The drag on the grids were measured using the force balance in the Donald Campbell wind tunnel (see http://www3.imperial.ac.uk/vortexflows/experimentalfacilities/donaldcampbellwindtunnel/).

3 The mixing elements

Firstly, two fractal grids were considered - termed herein FG1 and FG2. Both grids were based on a closed square contour repeated at 4 different scales (see figures 1 herein and figure 32 in Hurst & Vassilicos 2007).

The ratio t_r of the thickness of the largest to smallest square and the blockage ratio σ were varied between the fractal grids. For FG1, $t_r = 10.8$ and $\sigma = 30.5\%$; for FG2, $t_r = 15.6$ and $\sigma = 38.5\%$. For comparison, the similarly shaped fractal square grids used by Hurst & Vassilicos (2007), Seoud & Vassilicos (2007a,b,c) and Mazellier *et al.* (2007a,b) in their wind tunnel experiments have values of t_r ranging between 2.5 and 28, $\sigma = 25\%$ and are twice or four times larger because their wind tunnels' width is twice and four times greater than our flume's width.

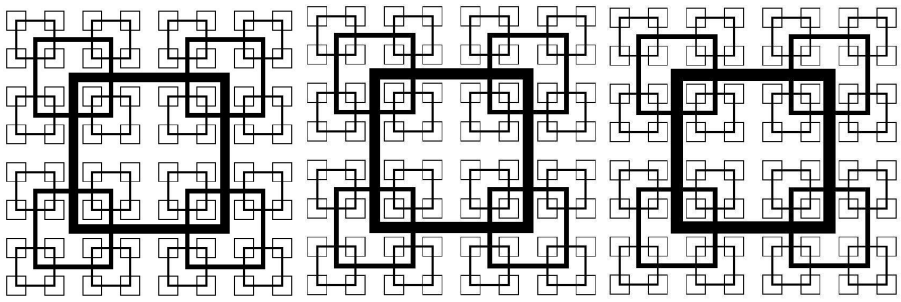

(a) $t_r = 8.5$ (b) $t_r = 13.0$ (c) $t_r = 17.0$

Figure 1: Fractal square grids used by Hurst & Vassilicos (2007) for which all parameters are equal except the thickness ratio t_r which is, from left to right, $t_r = 8.5, 13.0, 17.0$.

Secondly, two pattern-enhanced fractal grids (PEFG1 and PEFG2) were considered which are not shown here because, unlike FG elements, they have not been patented. The blockage ratio of PEFG2 is a little bit higher than the blockage ratio of PEFG1.

These fractal grids were compared to the current industrial state of the art for some static inline mixers, here refered to as CSM element and, as a point of reference, to a comparable regular turbulence-generating grid with $\sigma = 34\%$. It may be worth noting that the turbulence intensity and pressure drop generated by regular grids cannot be varied independently; both quantities increase with blockage ratio much faster than linearly, but blockage ratios appreciably higher than the present one result in significantly inhomogeneous turbulence and very high pressure drops (Corrsin 1963). The pressure drop across this grid is significantly higher than across the fractal grids used by Hurst & Vassilicos (2007) and it generates turbulence intensities significantly lower than these fractal grids.

We also compared with the base case where there is no mixing element.

4 Comparative Measures

Focus was on direct comparisons between the mixers based on the time-averaged concentration fields, Coefficients of Variance (CoV) and the drag across the mixers.

The Cartesian coordinates x, y, z correspond to streamwise distance x from the mixing element, distance within the depth of camera view y (this is a horizontal distance in the experiment) and spanwise distance z from the centreline (this is a vertical distance in the experiment). Dye was continuously released from a point source at various positions and we denote the concnetration $c(x, y, z, t)$. Our dye-attenuation measurements access the instantaneous values $C(x, z, t) = \int c(x, y, z, t)dy$ rather than $c(x, y, z, t)$ because they effectively integrate over the depth of camera view. These depth-averaged concentrations are presented herein in the form of a time-averaged normalised concentration field

defined by

$$\bar{C}(x,z) = \frac{\int C(x,z,t)\,\mathrm{d}t}{\frac{1}{L}\iint C(x,z,t)\,\mathrm{d}t\mathrm{d}z} \tag{1}$$

Here, L is the vertical extent of the test section (in this case $L = 20$ cm). The time-averages were formed from 1200 measurements (obtained by taking 6 measurements per second for 200 seconds) and the integrals in the z direction were calculated from profiles of C containing approximately 500 measurements (measured over the 20 cm vertical extent test section).

In order to directly compare mixing quality with a single measure, a time-averaged Coefficient of Variance (CoV) was considered, formed by taking averages over time and over the spanwise distance z. This CoV may be defined as:

$$CoV_x = \frac{\sigma_x}{m_x} \tag{2a}$$

where

$$m_x = \frac{1}{L}\int \bar{C}(x,z)\,\mathrm{d}z \quad \text{and} \quad \sigma_x^2 = \frac{1}{L}\int \left(\bar{C}(x,z) - m_x\right)^2\,\mathrm{d}z. \tag{2b}$$

The subscript x reads 'time-averaged and z-averaged value at the downstream location x'.

5 Results

5.1 Drag across the mixers

In figure 5.1 we plot the drag on the fractal and CSM elements measured in the wind tunnel for different freestream velocities. The figure shows that the fractal elements suffer less drag than the CSM element and that the PEFG2 element suffers the same drag as the CSM element at freestream velocities U_∞ of the order of 10 m s^{-1} and below. The normalised drag, defined as the drag divided by ρU_∞^2 (where ρ is the density of air), of the FG1 and FG2 elements is 91% and 72% of the CSM's normalised drag. The normalised drag of the PEFG2 element is 105% of the CSM's normalised drag. The normalised drag of the PEFG1 element is lower than that of the PEFG2 element.

5.2 Mixing quality measured in terms of a single CoV_x value at various downstream x distances

Figures 3 and 4 show how the coefficient of variance varies when the dye contaminant is released, respectively, upstream and downstream of the grid. Both the FG elements' CoV_x values are larger than the CSM's but nevertheless comparable in magnitude. This is already some success for the first try with a new type of unoptimised element when compared to a highly optimised widely tested and widely used top-performance commercial element.

We designed a new type of fractal grid, the pattern-enhanced fractal grids PEFG1 and PEFG2. PEFG1 was the first to be designed and constructed. When tested, it showed a very significant improvement to the non-enhanced fractal grids FG1 and FG2. In particular, in the near field it performs as well as the CSM element, though not in the far field. Our next try at a PEFG element,

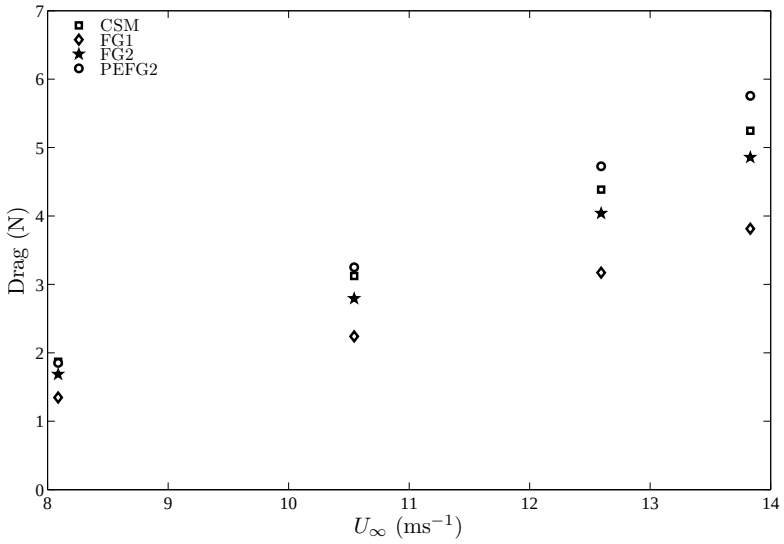

Figure 2: Drag across the mixers against the freestream velocity U_∞. The squares represent the CSM mixer, the diamonds FG1, the stars FG2 and the circles PEFG2.

even though unoptimised, gave rise to PEFG2 which mixes as well as the CSM in the far field and **better** than the CSM in the near field!

As shown in figure 5, combinations of PEFG2 and CSM (where CSM is placed downstream of PEFG2) mix even better than both individual PEFG2 and CSM elements and in fact mix very fast immeadiately downstream of the combination. Indeed, the CoV_x value decreases very abruptly across the CSM element when a PEFG2 element is placed upstream of the CSM. This is quite an extraordinary result.

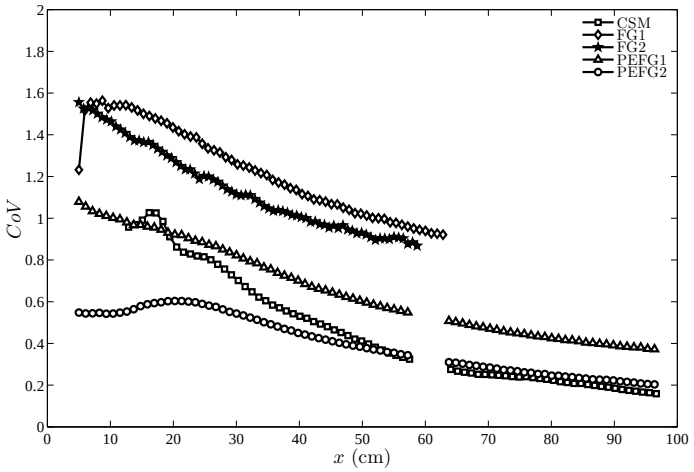

Figure 3: The coefficient of variance (CoV_x) when the dye source is upstream of the grid. These measurements relate to a dye release at $x = -30$ cm, $y = 0$ cm and $z = 0$ cm into a freestream velocity of $U_\infty = 29.3$ cms^{-1} .

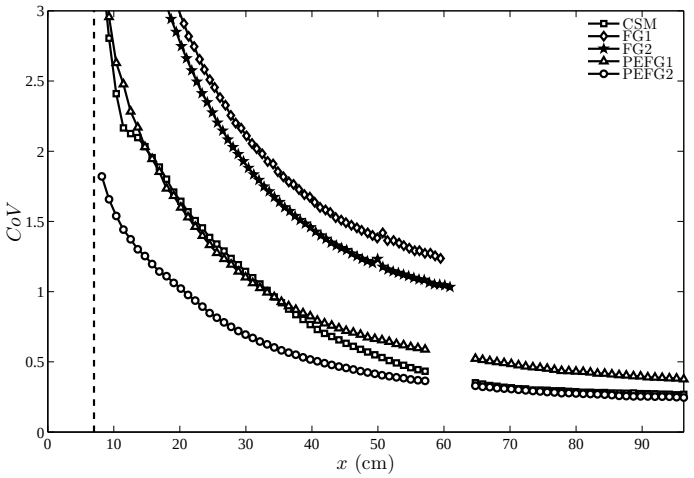

Figure 4: The coefficient of variance (CoV_x) when the dye source is downstream of the grid. These measurements relate to a dye release at $x = 7$ cm, $y = 0$ cm and $z = 0$ cm into a freestream velocity of $U_\infty = 29.3$ cms^{-1} .

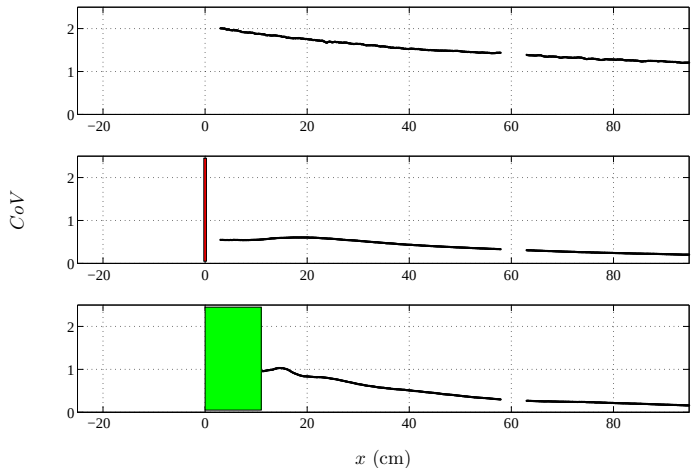

(a)

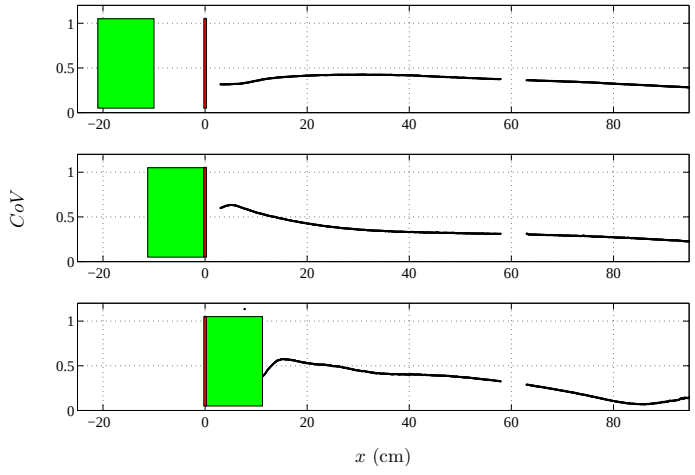

(b)

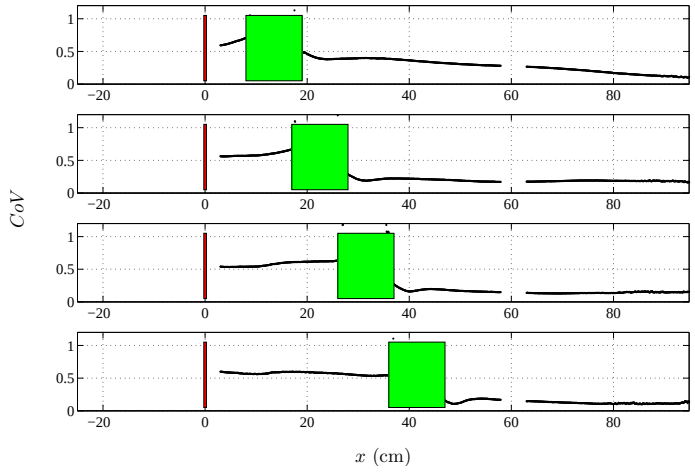

(c)

Figure 5: The coefficient of variance (CoV_x) when the dye source is upstream of the grid. These measurements relate to a dye release at $x = -30$ cm, $y = 0$ cm and $z = 0$ cm into a freestream velocity of $U_\infty \approx 25$ cms^{-1}. The thin red rectangle represents PEFG2 and the green retangle the CSM mixer.

5.3 Concentration fields and profiles

As a point of reference we first present the concentration fields for a dye release into a freestream, and a dye release into a freestream containing a regular rectangular grid, figure 6. We observe that the turbulence generated by the regular grid allows more rapid dilution of the dye and results in a slighter faster spread.

5.3.1 Individual mixers

The figures in this subsection show plots of the CoV dependence on the streamwise coordinate x, maps of the normalised time-averaged concentration ($\bar{C}(x,z)$) and plots of the z-distribution of $\bar{C}(x,z)$ at different downstream positions x. We have chosen a representative case where the dye is released upstream of the mixers at $x = -30$ cm. As a point reference, figure 7 shows the development of the concentration field in the absence of a mixing element in which case we observe a slow spreading of the dye, with the time-averaged concentration retaining a Gaussian-like profile. In figures 7–12 and figures 14–21 colours denote the normalised concentration values ($\bar{C}$) with values given on the colour bar.

Figure 8 shows these mixing statistics and concentration field map for the CSM element. We observe a more complex concentration field and clearly non-Gaussian profiles with strong evidence of the fluid being advected towards the walls of the test section. This seems to happen as a result of the CSM element attempting a large-scale brading action of the flow thereby advecting considerable portions of the dye to the walls. Different release locations lead to different walls being targeted.

Figures 9 and 10 show these mixing statistics and concentration field map for the FG elements. The spreading is of course faster than without an element and also than for the regular grid. Gaussian-like profiles are observed in all these cases with their spreading fastest for the FG elements, in particular FG2. The presence of these Gaussian profiles implies that there is no large-scale advection of fluid against the mean flow and that impact with the walls is, as a result, not used to enhance mixing.

Figures 11 and 12 show these mixing statistics and concentration field map for the PEFG elements. Unimodal and approximately symmetric profiles, as in FG cases, are observed but with a spread that is comparable to that of the profiles generated by the CSM. Good field homogeneity is achieved, particularly with the PEFG2 element, comparable to the homogeneity achieved by the CSM element in the far field but better in the near field. This is highlighted in figure 13 which directly compares the normalised concentration profiles of the CSM and PEFG2 mixers.

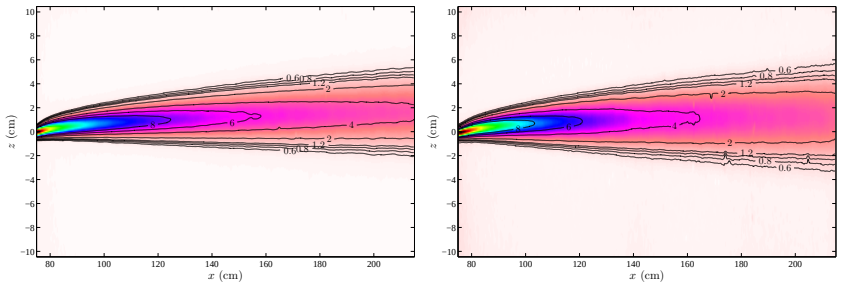

(a) No mixer (b) Regular rectangular grid

Figure 6: The time-averaged normalised concentration $\bar{C}$ with (a) no mixer and (b) a regular rectangular grid placed at $x = 0$ cm. Dye was released at $x = 75$ cm, $y = 0$ cm and $z = 0$ cm into a horizontal mean flow ($U_\infty = 29.3$ cms^{-1}).

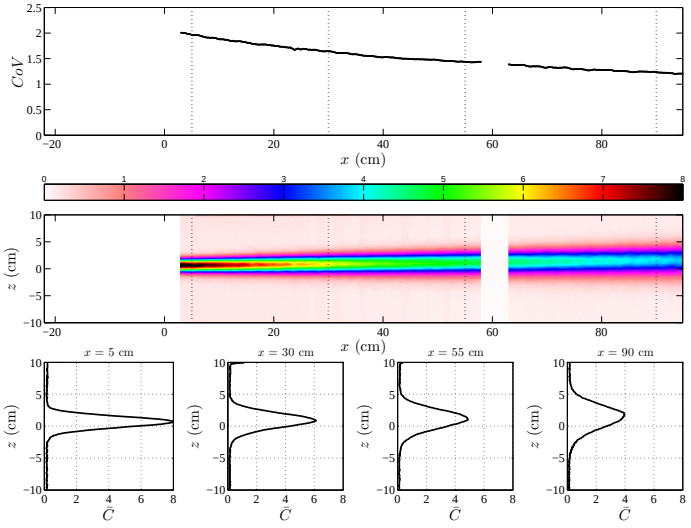

Figure 7: **No Grid:** The coefficient of variance and normalised concentration fields when the dye source is upstream of the grid. These measurements relate to a dye release at $x = -30$ cm into a freestream velocity of $U_\infty \approx 25$ cms^{-1}. In this case there is no inline mixer (and as such results may be used as a point of reference for contrast with the following figures).

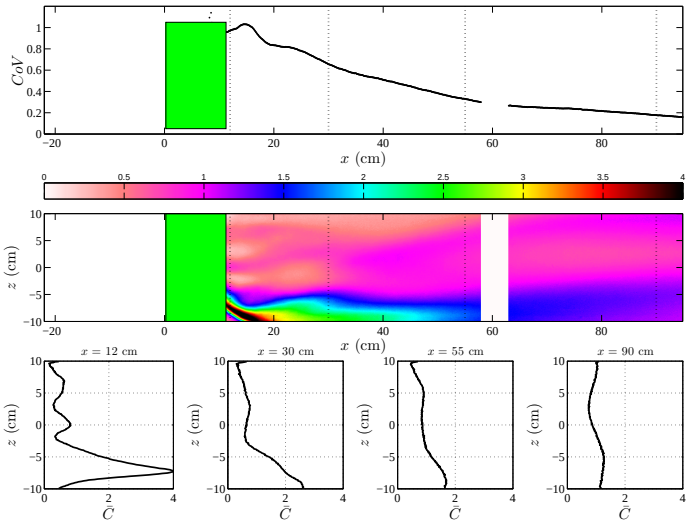

Figure 8: **CSM:** The coefficient of variance and normalised concentration fields when the dye source is upstream of the grid. These measurements relate to a dye release at $x = -30$ cm into a freestream velocity of $U_\infty \approx 25$ cms^{-1}. The green rectangle represents the CSM mixer.

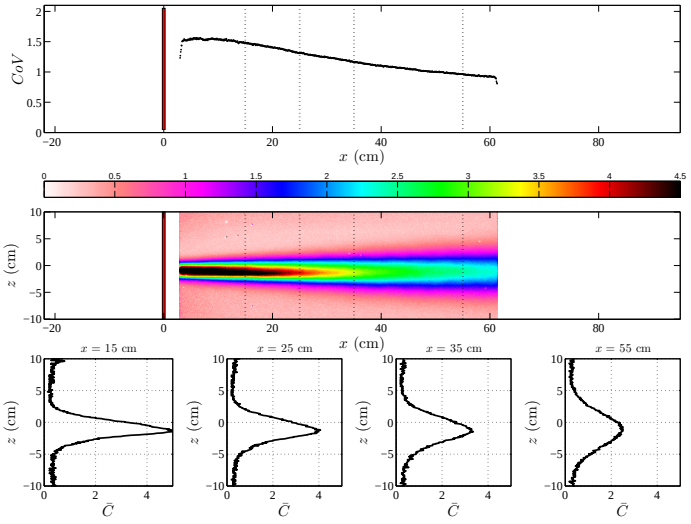

Figure 9: **FG1:** The coefficient of variance and normalised concentration fields when the dye source is upstream of the grid. These measurements relate to a dye release at $x = -30$ cm into a freestream velocity of $U_\infty \approx 25$ cms^{-1}. The red rectangle represents FG1.

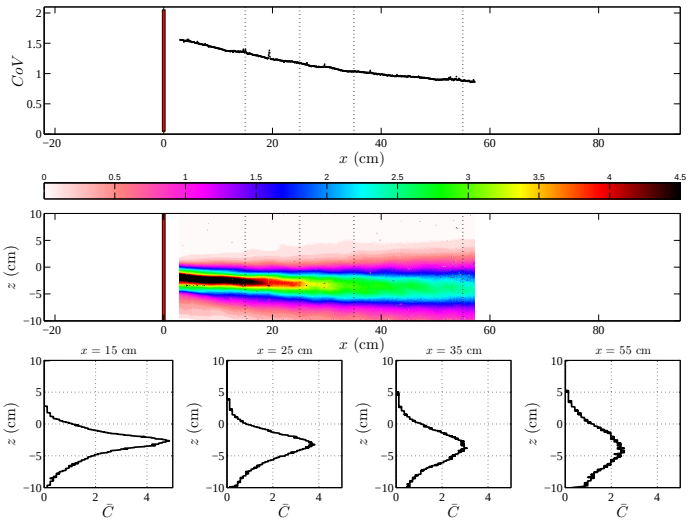

Figure 10: **FG2:** The coefficient of variance and normalised concentration fields when the dye source is upstream of the grid. These measurements relate to a dye release at $x = -30$ cm into a freestream velocity of $U_\infty \approx 25$ cms^{-1}. The red rectangle represents FG2. Note the asymmetry. A property of the fractal mixers is that they tend to exagerate any underlying asymmetry — in this experiment the nozzle was place at $z \approx -0.1$ cm.

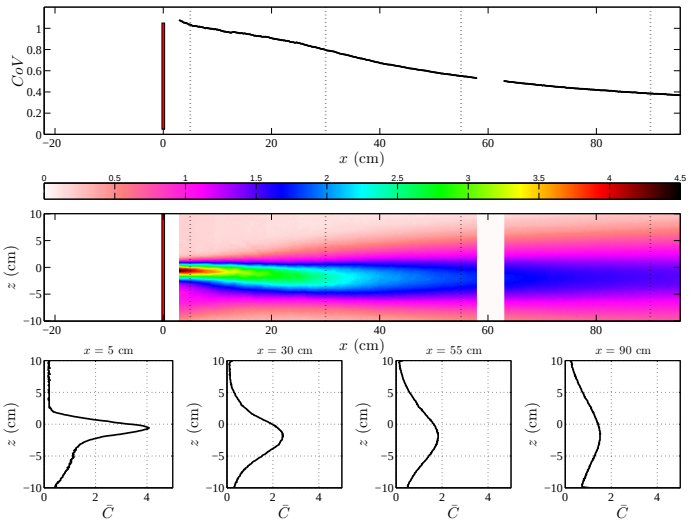

Figure 11: **PEFG1:** The coefficient of variance and normalised concentration fields when the dye source is upstream of the grid. These measurements relate to a dye release at $x = -30$ cm into a freestream velocity of $U_\infty \approx 25$ cms^{-1}. The red rectangle represents PEFG1.

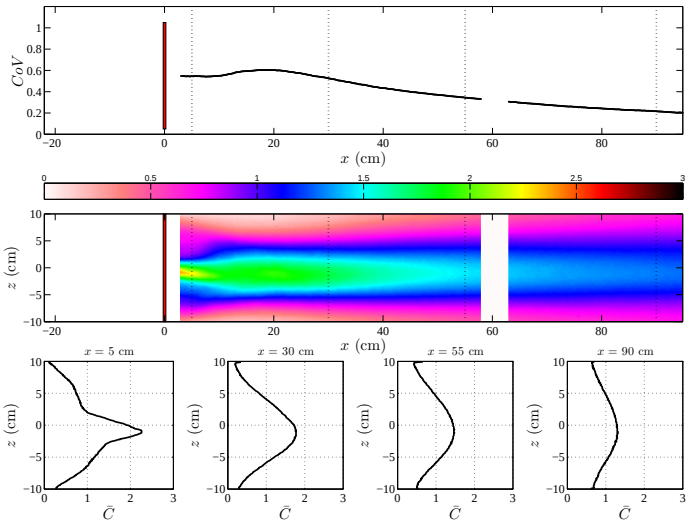

Figure 12: **PEFG2:** The coefficient of variance and normalised concentration fields when the dye source is upstream of the grid. These measurements relate to a dye release at $x = -30$ cm into a freestream velocity of $U_\infty \approx 25$ cms^{-1}. The red rectangle represents PEFG2.

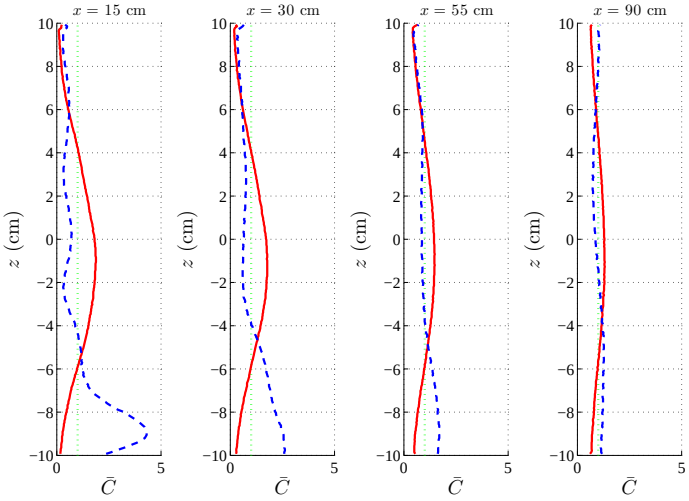

Figure 13: A comparison of the normalised concentration profiles ($\bar{C}$) between the CSM mixer and PEFG2 mixer. The blue dashed line represents the CSM mixer and the red the PEFG2 mixer. The green dotted line shows the normalised concentration profile if the dye were mixed uniformly throughout the tunnel.

5.3.2 Coupled mixers

The PEFG2 is a better mixing element than the CSM in the near field where most of its turbulent stirring and mixing action lies. This early mixing action is so vigorous and effective that the mixing by the PEFG2 turns out to be nearly identical in terms of CoV_x to the mixing by the CSM in the far field even though the PEFG2 does not sustain much action in the far field. The CSM mixes by generating large scale motions which therefore take a long time or distance downstream to be fully effective. A drawback of these large scale motions is their use of the walls to generate the mixing. These observations can be quite clearly made from the figures of the previous subsection.

As a result of these observations one might expect the combination CSM-PEFG2 where the CSM is placed upstream of the PEFG2 to return lower quality mixing than the combination PEFG2-CSM where it is the PEFG2 which is placed upstream of the CSM. This is indeed what is observed. What is more, we find that the PEFG2-CSM combination returns an exceptionally good mixing performance, much better than both individual CSM and PEFG2 stirrers and also much better than the combination CSM-CSM of two CSM elements. The figures supporting these conclusions are in this subsection. Within the limitations of the present report, we have not been able to test PEFG2-PEFG2 or other fractal-fractal combinations. We can expect such optimised combinations of optimised PEFG elements with optimised release strategies to generate a new standard of very high quality mixing with exceptionally low CoV_x values, homogeneous concentration maps and profiles as well as little action on the walls — all this at a very short distance downstream from the mixing elements. The technology is generic and should be adaptable to a wide range of applications with different optimisations for each.

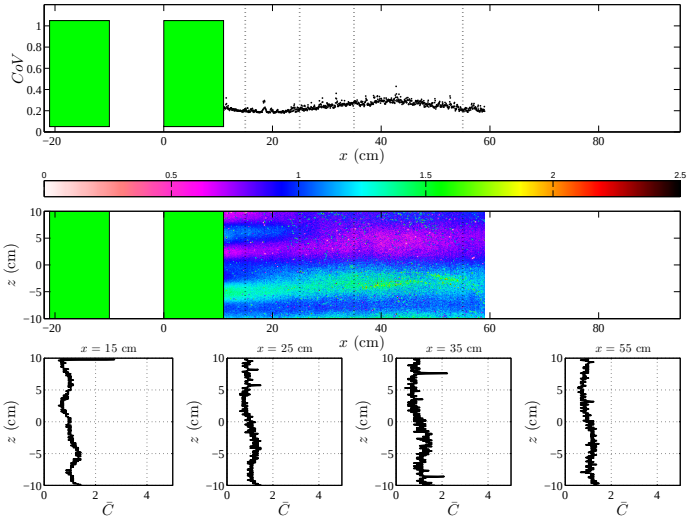

Figure 14: **CSM-CSM:** The coefficient of variance and normalised concentration fields when the dye source is upstream of the grid. These measurements relate to a dye release at $x = -30$ cm into a freestream velocity of $U_\infty \approx 25$ cms^{-1}. The green rectangles represent CSM mixers.

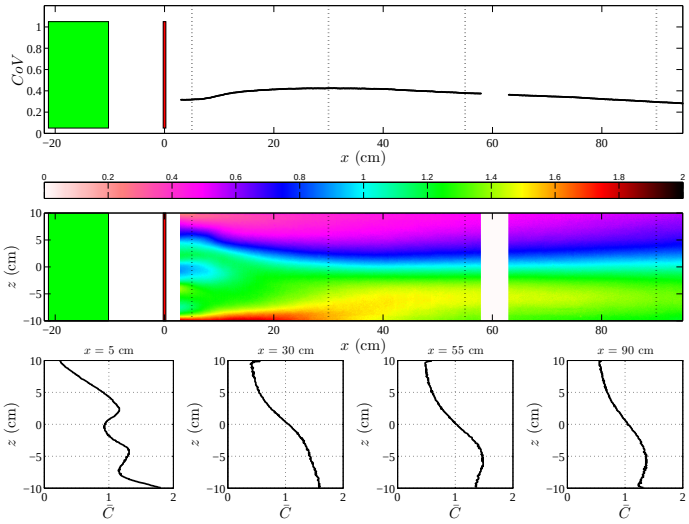

Figure 15: **CSM-PEFG2:** The coefficient of variance and normalised concentration fields when the dye source is upstream of the grid. These measurements relate to a dye release at $x = -30$ cm into a freestream velocity of $U_\infty \approx 25$ cms^{-1}. The red rectangle represents PEFG2 and the green rectangle the CSM mixer.

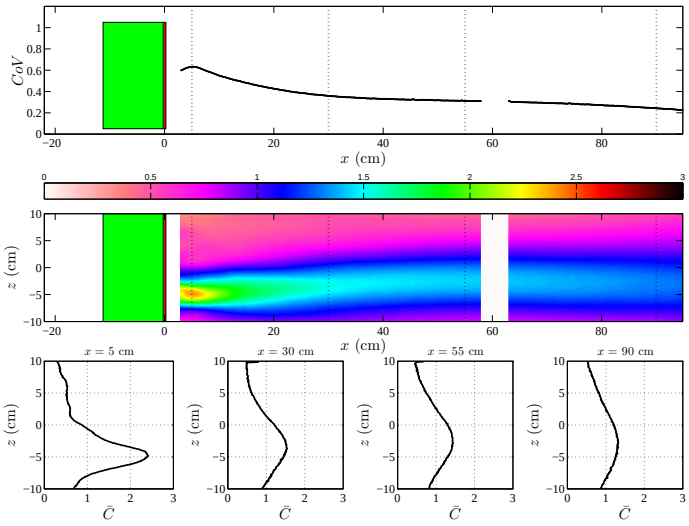

Figure 16: **CSM-PEFG2:** The coefficient of variance and normalised concentration fields when the dye source is upstream of the grid. These measurements relate to a dye release at $x = -30$ cm into a freestream velocity of $U_\infty \approx 25$ cms^{-1}. The red rectangle represents PEFG2 and the green rectangle the CSM mixer.

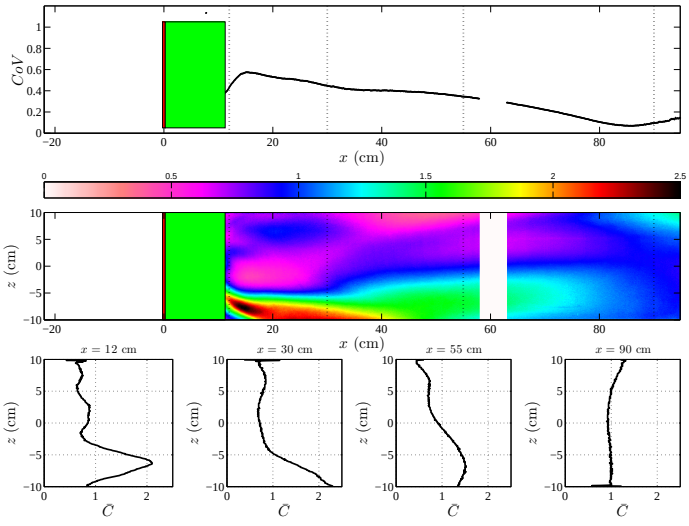

Figure 17: **PEFG2-CSM:** The coefficient of variance and normalised concentration fields when the dye source is upstream of the grid. These measurements relate to a dye release at $x = -30$ cm into a freestream velocity of $U_\infty \approx 25$ cms^{-1}. The red rectangle represents PEFG2 and the green rectangle the CSM mixer.

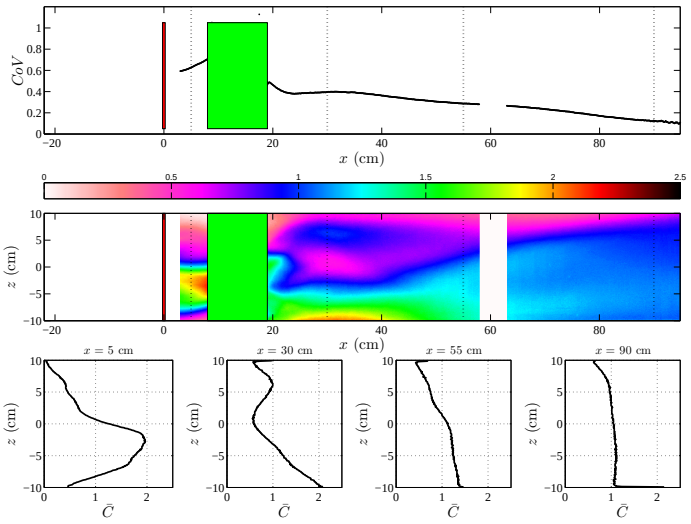

Figure 18: **CSM-PEFG2:** The coefficient of variance and normalised concentration fields when the dye source is upstream of the grid. These measurements relate to a dye release at $x = -30$ cm into a freestream velocity of $U_\infty \approx 25$ cms^{-1}. The red rectangle represents PEFG2 and the green rectangle the CSM mixer.

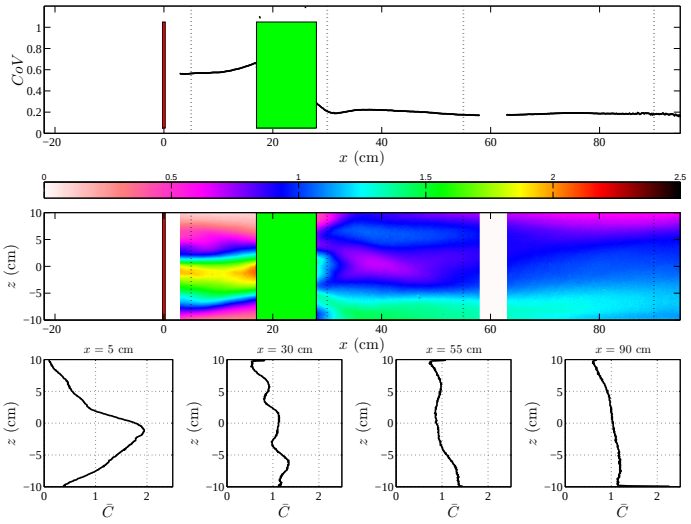

Figure 19: **CSM-PEFG2:** The coefficient of variance and normalised concentration fields when the dye source is upstream of the grid. These measurements relate to a dye release at $x = -30$ cm into a freestream velocity of $U_\infty \approx 25$ cms^{-1}. The red rectangle represents PEFG2 and the green rectangle the CSM mixer.

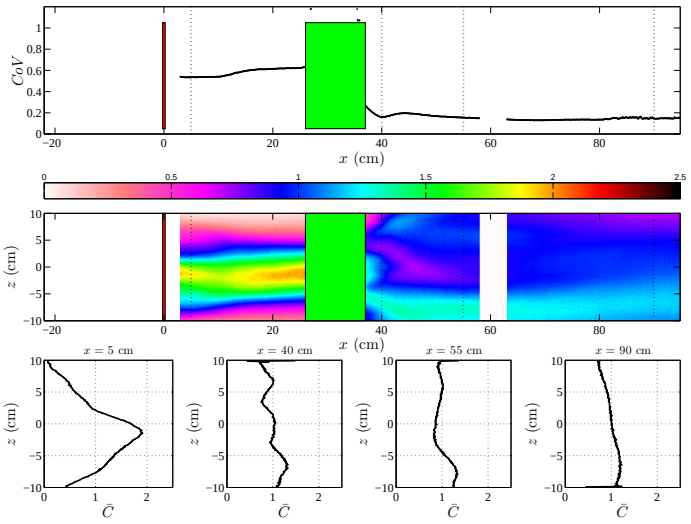

Figure 20: **CSM-PEFG2:** The coefficient of variance and normalised concentration fields when the dye source is upstream of the grid. These measurements relate to a dye release at $x = -30$ cm into a freestream velocity of $U_\infty \approx 25$ cms^{-1}. The red rectangle represents PEFG2 and the green rectangle the CSM mixer.

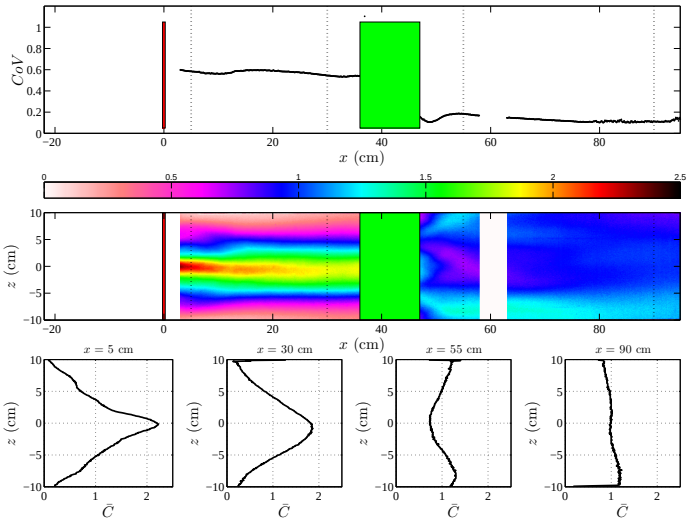

Figure 21: **CSM-PEFG2:** The coefficient of variance and normalised concentration fields when the dye source is upstream of the grid. These measurements relate to a dye release at $x = -30$ cm into a freestream velocity of $U_\infty \approx 25$ cms^{-1}. The red rectangle represents PEFG2 and the green rectangle the CSM mixer.

6 Conclusions

Our main conclusions are itemised below. With the obvious exception of our results on drag, they have been obtained for continuous point releases of dye concentrations.

- The CoV_x values and local time-averaged concentration values achieved by the CSM element are generally lower than those achieved by the fractal and regular grids. However, they are higher in the near field and about equal in the far field to the respective values achieved by the PEFG2 element.

- The CSM element seems to rely on the walls for its far field mixing levels. Two CSM elements in tandem mix particularly well, but not as well as the combination PEFG2-CSM with the CSM upstream of the PEFG2. The fractal grids mix by generating high turbulence levels and are therefore able to keep the mixing activity and the concentration field clear from the walls. Fractal grids mix far better than regular grids which also mix by generating turbulence. They both achieve their mixing in the near field and not far downstream whereas the CSM achieves most of its good mixing far downstream.

- Mixing effectiveness is a function of both mixing quality and the necessary power input to achieve it. Single FG elements result in significantly less drag and consequent less power loss than single CSM elements and single regular grids. Where many mixing elements are used, the economy in power input brought by the use of fractal grids will be even greater. Current unoptimised single PEFG elements result in similar drag as single CSM elements.

- In conclusion, fractal grids mix relatively well by generating disproportionately high turbulence intensities for the pressure drop they cause. In doing so, they keep the mixing activity clear from the walls and close to the grid. With further design/development and resolving grid manufacturing constraints it should be possible to improve fractal mixing without increasing, and sometimes even further decreasing, power losses. Considering the design constraints on fractal grids detailed in Hurst & Vassilicos (2007), this should be particularly easy to achieve for larger mixers. It should be enough to scale up fractal grids such as those used here but improved with (lower) values of σ and (higher) values of t_r. Smaller mixers can also be considered and more design parameters can be varied to address them, all of which are detailed in Hurst & Vassilicos (2007). For example, of interest to both large and small mixers, many different shapes may be considered (round, rectangular, *etc.*) as well as different materials for its construction, including metals and plastics. The distance downstream from fractal grids where the turbulence intensity peaks independently of flow velocity can be adjusted by adjusting the ratio of the largest length to the largest thickness on the fractal square grid (Mazellier *et al.* (2007b). This is yet another parameter distinct from and independent of t_r and σ, and it has bearing on the distance downstream where mixing is achieved. Where uniform mixing is required throughout the volume of the duct, various

combinations of CSM and fractal elements may be considered which can achieve uniformity without overloading the duct's walls.

- Different mixers operate with different injection modes and the optimised injection procedure for different fractal mixers consisting of one or more fractal elements of different types, combined or not with other mixing elements such as the CSM one, are yet to be determined. Different applications may require different fractal mixers.

- Last but not least, we note that the methodology applied herein, namely of non-intrusive evaluations of tracer concentration fields in conjunction with detailed flow visualisation, readily enables the properties and behaviour of static inline mixers to be quantified. This, in turn, enables a systematic approach to effective mixer engineering and optimisation.

References

Corrsin, S. 1963 Turbulence: experimental methods. In *Handbook der Physik*, 524.

Dalziel, S. B. 1992 Rayleigh-Taylor instability: experiments with image analysis. Dyn. Atmos. Oceans **20** 127–153

Hacker, J., Linden P. F. & Dalziel, S.B. 1996 Mixing in lock-release gravity currents. Dyn. Atmos. Oceans **24** 183 – 195

Hurst, D. & Vassilicos, J.C. 2007 Scalings and decay of fractal-generated turbulence. Phys. Fluids **19** (3)

Mazellier, N., Bruera, C., Baudet, C. & Vassilicos, J.C. 2007a Production turbulente en aval d'une grille fractale. Proceedings of the 18th Congres Francais de Mecanique, Grenoble, 27-31 August 2007.

Mazellier, N., Bruera, C. & Vassilicos, J.C. 2007b The flow topography in the turbulence production region generated by fractal square grids. Preprint in preparation.

Seoud, R.E. & Vassilicos, J.C. 2007a Passive multiscale flow control by fractal grids. In Proceedings of the IUTAM Symposium on Flow Control and MEMS, London, U.K., 19-22 September 2006.

Seoud, R.E. & Vassilicos, J.C. 2007b Turbulence generated by fractal grids in the wind tunnel. In Proceedings of the 11th EUROMECH European Turbulence Conference, Porto, Portugal, 25-28 June 2007.

Seoud, R.E. & Vassilicos, J.C. 2007c Dissipation and decay of fractal-generated turbulence. Preprint (2007b).